ICIC Express Letters
Part B: Applications
Volume **8**, Number **3**, March **2017**

ICIC International ©2017 ISSN 2185-2766
pp. **469–476**

DEVELOPMENT OF A NOVEL HIGH STEP-DOWN CORRECTION MAGNET POWER SUPPLY WITH PHOTOVOLTAIC SYSTEM

Yong-Seng Wong, Kuo-Bin Liu*, Chen-Yao Liu, Yuan-Chen Chien and Bao-Sheng Wang

Department of Power Supply Group
National Synchrotron Radiation Research Center
No. 101, Hsin Ann Road, Hsinchu 300, Taiwan
wong.ys@nsrrc.org.tw; *Corresponding author: kbl@nsrrc.org.tw

Received August 2016; accepted November 2016

Abstract. *This study simulates a high step-down gain DC-DC converter that integrates a buck-type converter and isolated transformer. Isolated transformer turn ratio and main power switch duty cycle are used to adjust the output voltage. This paper integrates coupled inductor and switch capacitor to achieve a high step-down voltage gain without extreme duty cycle. Coupled inductor has a clamp diode and clamp capacitor can recover energy by leakage inductor. Therefore, the voltage stress on the main power switch can be reduced and low voltage stresses components were selected. In this proposed system, the converter is composed of one main switch, one isolated transformer, two capacitors, and two diodes. Continuous conduction mode operation and formula derivation are discussed. Finally, Simplis software is used to simulate an input voltage of 24 V to output voltage of 5 V and correction magnet power converter of 50 W. Detailed current and voltage waveforms are provided and verified by the simulation result.*
Keywords: High step-down, Photovoltaic system, Light source, Correction magnet power supply

1. **Introduction.** In the 21st century, synchrotron radiation can analyze many unsolved mysteries of science, such as protein, DNA, and semiconductor molecular structures. Experiments using synchrotron radiation attempt to analyze electrons, photons, and other particles that are emitted when synchrotron radiation strikes matter. The resulting data are used to deduce the chemistry, geometry, electronic structure, or magnetic properties of matter. On radiology, proton therapy machines are widely used in the treatment of cancer cases, and high-precision proton knife is used to remove tumor from patients. Compared with conventional X-ray radiotherapy or Gamma Knife, proton knife treatment causes less damage to surrounding normal cells and fewer side effects; thus, proton knife therapy is currently the world's most advanced radiation oncology technology [1,2].

Synchrotron radiation or proton therapy machines are required to have a storage ring power supply to ensure electronic operation at the speed of light. After reaching the target energy, the electrons are transferred from the booster ring to the storage ring through a transport line. A series of magnets situated around the ring steers the electrons along circular arcs, and synchrotron radiation is continuously emitted tangentially from the arcs. Storage ring correction magnet power supply provides energy to the storage ring corrector magnets to ensure optimal trajectory of the electron beam with the speed of light in a vacuum. Currently, storage ring correction power supply mainly uses AC-DC inverter architecture technology and phase-shift full-bridge converter with current doubling technology to transfer energy to the magnet. This circuit must use multiple switches and generates a high voltage stress caused by high switching losses in the switch; this storage ring power supply enables a technical efficiency of more than 90% [3].

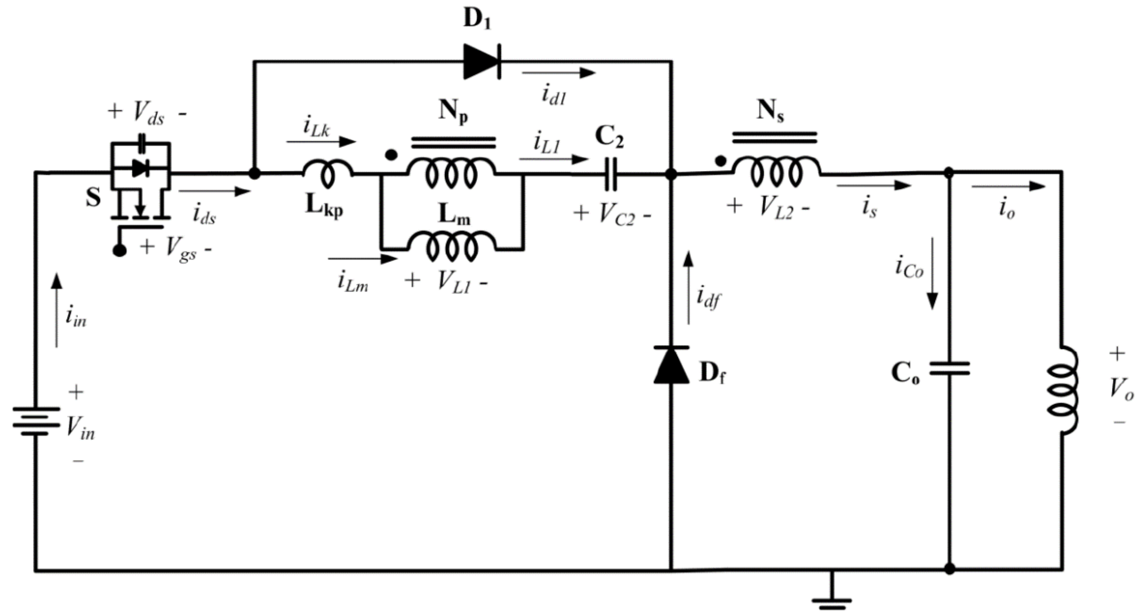

FIGURE 1. Proposed converter equivalent circuit

The output voltage of the solar module is a DC voltage; the energy conversion to the corrector magnet occurs through a DC-DC step-down converter. Early scholars focused on high step-down voltage gain circuit, such as coupled inductor [4-7] and interleaved technology [8-11]. Coupled inductor technology is often used by high step-down converter; the transformer can easily achieve high step-down ratio and is not limited by duty cycle. Nevertheless, the leakage inductor of the coupled inductor will cause a high voltage spike when the switch is turned off. Many snubber circuits have been proposed to solve the voltage spike problem, but these circuits increase the number of components and reduce the efficiency of the power converter. The interleaved buck converter requires no transformer, but needs to increase the switch and passive components to achieve high step-down ratio. In this study, a novel switched capacitor buck converter is proposed. The novel switched capacitor buck converter equivalent circuit is shown in Figure 1. The PV system is the input source; v_{in} and i_{in} are the current and voltage of PV respectively, and the voltage of the PV system is based on the brightness of sunlight. The power switch is a high-frequency NMOSFET, and i_{ds} and v_{ds} are the flowing current and voltage, respectively. N_p: N_s is the proportion of step-down isolated transformer primary winding and secondary winding, and the turn ratio is $N_p : N_s = 1 : 3$. L_m and L_{kp} are the magnetizing and leakage inductors, respectively; switch capacitor (C_s) is the small volume that can easily obtain step-down voltage conversion ratio, and v_{cs} is the stress voltage of the switch capacitor. Switch capacitor releases energy via diode (D_1) and the flow current of D_1 is called i_{d1}. Freewheel diode (D_f) and secondary winding are serially connected with output correction magnet load; i_s and i_o are the current flow of the secondary winding and correction magnet, respectively. Continuous conduction mode (CCM) operation will be discussed in Section 2 and steady-state analysis will be presented in Section 3. Simplis simulation software experimental result of the proposed converter will be presented in Section 4 and the conclusion will be provided in Section 5.

2. **CCM Operation.** This proposed circuit has five modes of operation in period switching. Figure 2 shows each operation mode current flow with equivalent circuit of the proposed converter. Before the analysis of the operation mode, conditions are assumed to simplify the analysis of the proposed circuit. (1) The main switch is ideal, but the parasitic capacitor of the switch is not neglected. (2) All diodes are ideal. (3) The switch

capacitor (C_s) and output capacitor (C_o) are large. Therefore, v_{cs} and v_o are defined as the constant voltage in an operation mode. (4) Turn ration is defined as that n is equal to n_p/n_s.

Mode 1 $[t_0 - t_1]$: At this interval, the power switch is turned on. The PV system and inductor L_1 supply energy to capacitor C_s and inductors L_2 and L_m. The current of leakage inductor i_{Lk} and capacitor voltage V_{cs} is linearly increased and the current of magnetizing inductor i_{Lm} is linearly decreased. This mode ends when the inductor current $i_{L1} = 0$. D_1 and D_f show reverse bias. Current flow of this mode is shown in Figure 2(a).

Mode 2 $[t_1 - t_2]$: At this interval, the power switch is turned on. Capacitor C_s releases energy to inductor L_2 and PV system via diodes D_1 and D_f. Magnetizing inductor L_1 supplies energy to capacitor C_o; the current of leakage inductor i_{Lk} and magnetizing inductor i_{Lm} is linearly increased. This mode ends at $t = t_2$ when the power switch S is turned off. Current flow of this mode is shown in Figure 2(b).

Mode 3 $[t_2 - t_3]$: At this interval, the power switch is turned off. Capacitor C_s releases energy to inductor L_2, PV system and switch parasitic capacitor C_c via diodes D_1 and D_f. Magnetizing inductor L_1 supplies energy to capacitor C_o; the current of leakage inductor i_{Lk} and magnetizing inductor i_{Lm} is linearly increased. This mode ends at $t = t_3$ when the switch parasitic capacitor V_{CC} is fully charged with energy by capacitor C_s. Current flow of this mode is shown in Figure 2(c).

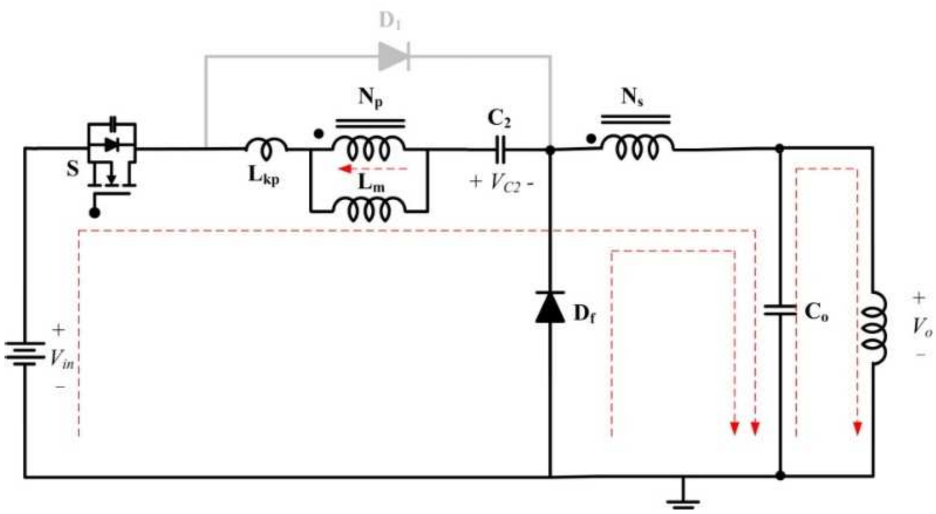

(a)

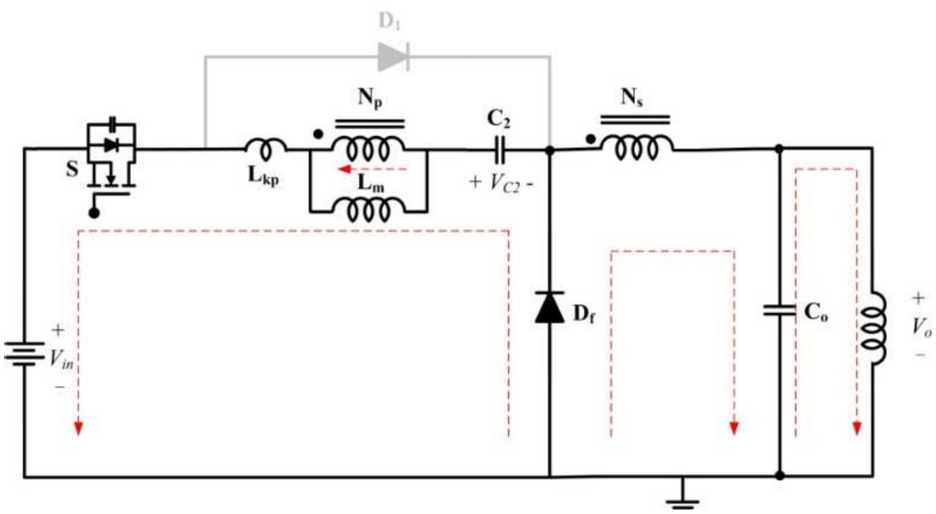

(b)

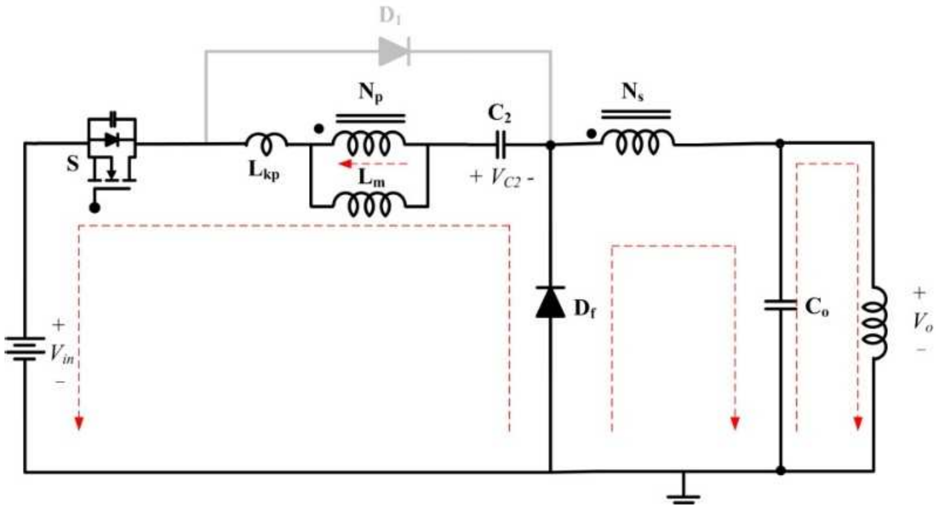

(c)

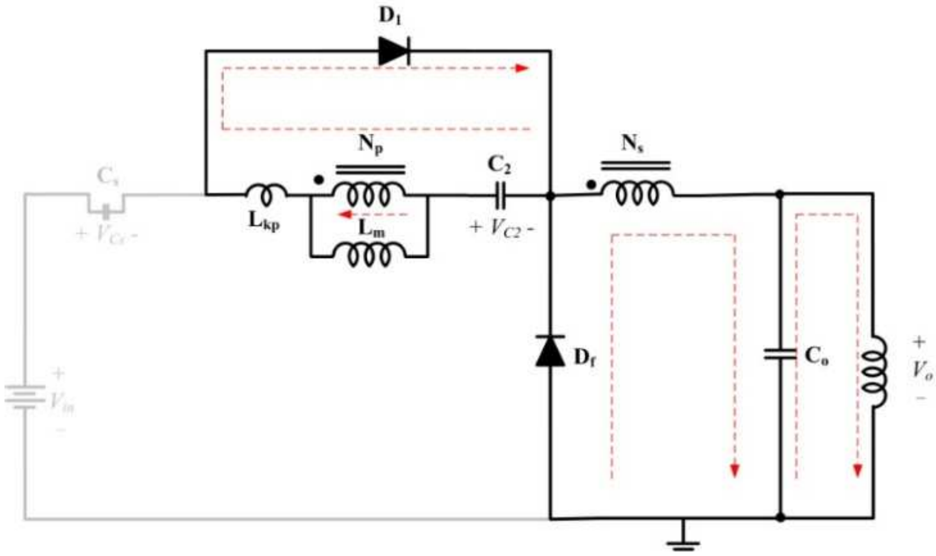

(d)

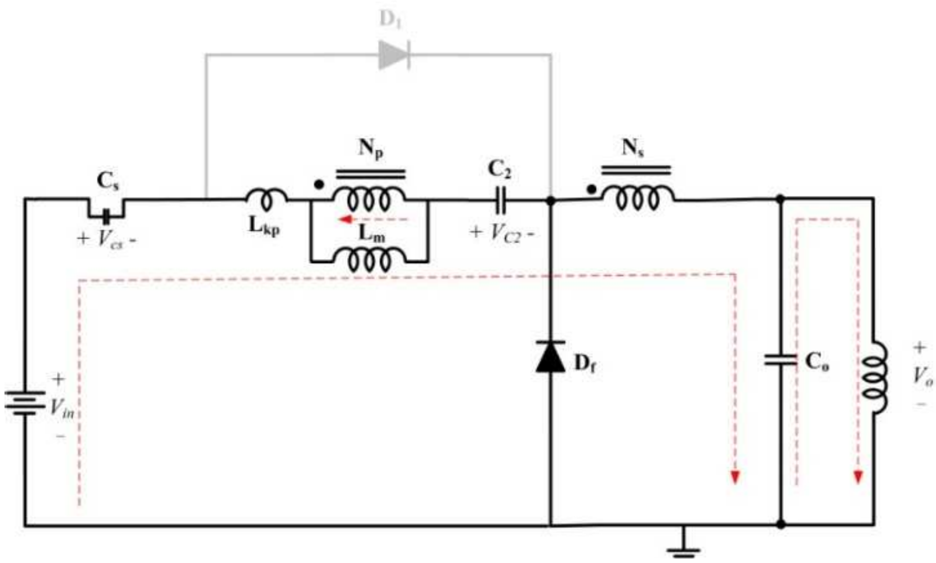

(e)

FIGURE 2. Operating modes during a switching period: (a) mode 1, (b) mode 2, (c) mode 3, (d) mode 4, and (e) mode 5

Mode 4 $[t_3 - t_4]$: At this interval, the power switch is turned off, and the parasitic capacitor is fully charging. Capacitor C_s releases energy to inductor L_2 via diode D_1, magnetizing inductor L_1 supplies energy to capacitor C_o via diode D_f and the current of leakage inductor i_{Lk} and magnetizing inductor i_{Lm} is linearly decreased. This mode ends at $t = t_4$ when capacitor C_s is an empty energy. Current flow of this mode is shown in Figure 2(d).

Mode 5 $[t_4 - t_5]$: At this interval, the power switch is turned off. Inductors L_2, L_1, L_m, and switch parasitic capacitor C_c release energy to capacitors C_s and C_o. The current of leakage inductor i_{Lk} and magnetizing inductor i_{Lm} is linearly decreased. This mode ends at $t = t_5$ when the power switch is turned on. Current flow of this mode is shown in Figure 2(e).

3. Steady-State Analysis.

Modes 1, 3, and 4 are ignored to simplify the analysis process. These operation modes present a short switching period. Modes 2 and 5 will be conceded in this section.

Before the analysis of modes 2 and 5, the turn ratio n and coupling coefficient k of the coupled inductor is defined as follows:

$$n = \frac{N_s}{N_p}, \tag{1}$$

$$k = \frac{L_m}{L_m + L_{kp}}. \tag{2}$$

From Kirchhoff's voltage law, the equations for voltage of inductors L_{kp} and L_2 at mode 2 and input voltage can be derived as follows:

$$V_{Lkp(II)} = V_{Lp(II)}(1 - k_p)/k_p, \tag{3}$$

$$V_{Ls(II)} = -V_{Lp}/n, \tag{4}$$

$$V_{in} = V_{c2} + V_{Lp(II)}(1 - k_p)/k_p + V_{Lp(II)} + V_{Ls(II)} + V_o. \tag{5}$$

Substituting Equations (3) and (4) into Equation (5), voltage of L_1 equation can be written as follows:

$$V_{Lp(II)} = \frac{n(k_p)(V_{in} - V_{c1} - V_o)}{n - k_p}. \tag{6}$$

Voltage of inductor L_1 at mode 5 equation can be derived as follows:

$$V_{Lp(V)} = -V_{c2}. \tag{7}$$

The smaller L_k than L_m is neglected and the coupling coefficient k is equal to 1 to simplify the steady-state analysis. Modes 1, 3, and 4 are short and ignored by one switching cycle. The time intervals of modes 2 and 5 are considered. From the inductor volt-second balance principle, the inductor voltage must be zero in the steady-state operation in a period of an inductor:

$$\int_0^{DT_s} V_{L1}^{II} dt + \int_{DT_s}^{T_s} V_{L1}^{V} dt = 0. \tag{8}$$

Therefore, substituting Equations (6) and (7) into Equation (8), the inductor of L_1 equation can be obtained as follows:

$$\frac{n(V_{in} - V_{c1} - V_o)}{n - 1} D + (-V_{c2})(1 - D) = 0. \tag{9}$$

The voltage gain G_v of the proposed step-down converter can be represented as follows:

$$G_v = V_o/V_{in} = \frac{D}{n + 2D - 1}. \tag{10}$$

Figure 3 presents the duty cycle against voltage gain under different turn ratios of the proposed converter: turn ratio n = 2-5 and duty cycle D = 0-1. For this proposed

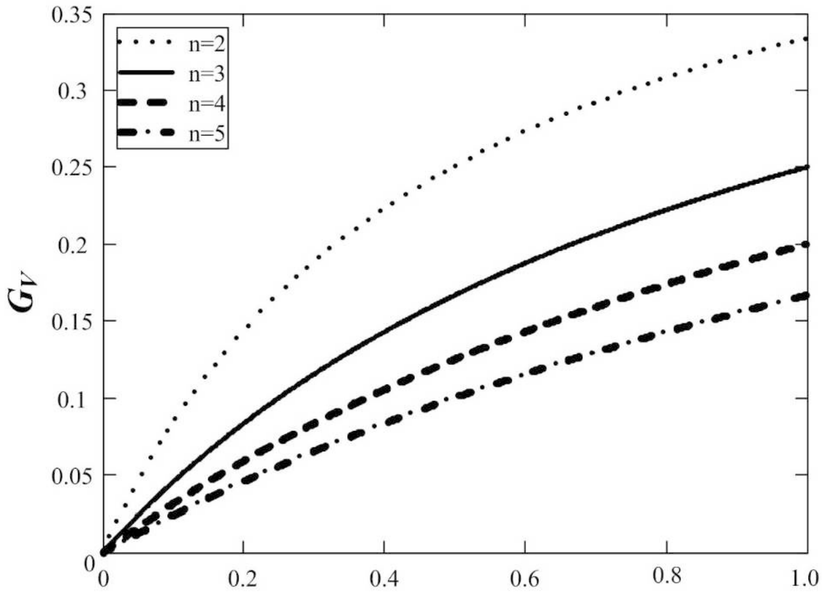

FIGURE 3. Duty cycle against voltage gain of the proposed converter

converter, the isolated transformer turn ratio is 3, the input voltage is 24 V, the output voltage is 5 V, and the step-down gain is appropriate 0.2. In the figure, the solid line denotes that $G_v = 0.2$ against a duty cycle that is appropriate $D = 0.7$.

4. **Simulation Result of the Proposed Converter.** A 50 W proposed converter is simulated, and its specifications are as follows:

1. Input DC voltage V_{in}: 24 V;
2. Output DC voltage V_o: 5 V;
3. Maximum output power: 50 W;
4. Switch frequency: 50 kHz;
5. Main switch: Ideal;
6. Diodes (D_1 and D_f): Ideal;
7. Capacitors: C_2: 20 μF/10 V, C_{o1}: 470 μF/10 V aluminum capacitors;
8. Transformer: N_p: $N_s = 1 : 3$, $L_m = 100$ μH, $L_{kp} = 0.3$ μH, $k = 0.997$.

The experimental voltage and current waveforms are presented in this section. The proposed converter has an input voltage of 24 V and output power of 50 W. The primary and secondary current against the gate-to-source voltage of the power switch is shown in Figure 4. The gate-to-source voltage is at a high level when the power switch is turned on; at this time, the primary and secondary inductor currents are increased to the maximum value. Otherwise, when $V_{gs} = 0$, the power switch is turned off, the primary inductor current becomes a negative current, and the secondary inductor current is decreased to release energy to output loading. Figure 5 shows the measured waveform of the capacitor voltage and output current at measurement capacitors C_2 and C_o voltage that can satisfy Equations (7) and (10) and output current of 10 A at full-load testing.

5. **Conclusion.** This study successfully simulated a high step-down gain DC-DC converter. The input source is a solar cell and the output loading is a correction magnet. The input voltage of 24 V decreases to the output voltage of 5 V, and the maximum output power is 50 W. This proposed converter uses an isolated transformer and coupled inductor to obtain a high step-down voltage gain. The proposed converter step-down gain can achieve a high step-down gain for the traditional buck converter. Coupled inductor

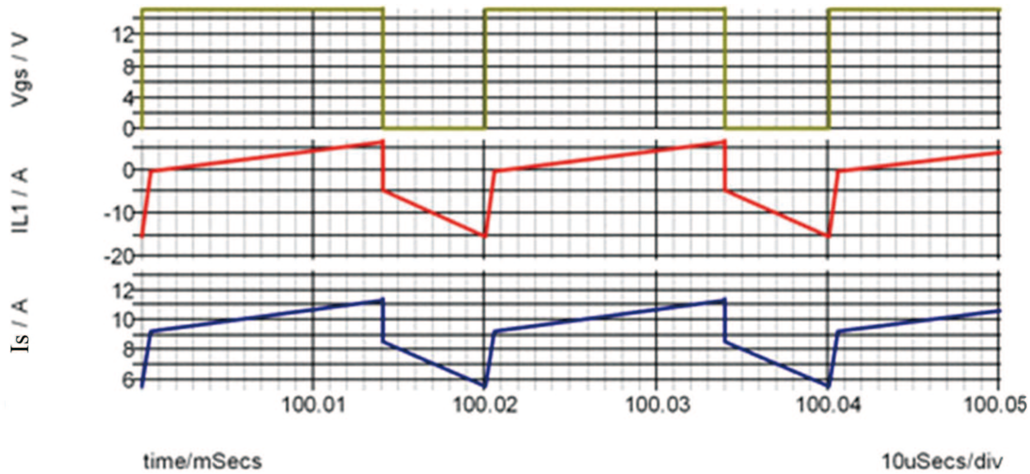

Figure 4. Simulation waveform of v_{gs}, i_{L1}, and i_s under full-load $P_o = 50$ W

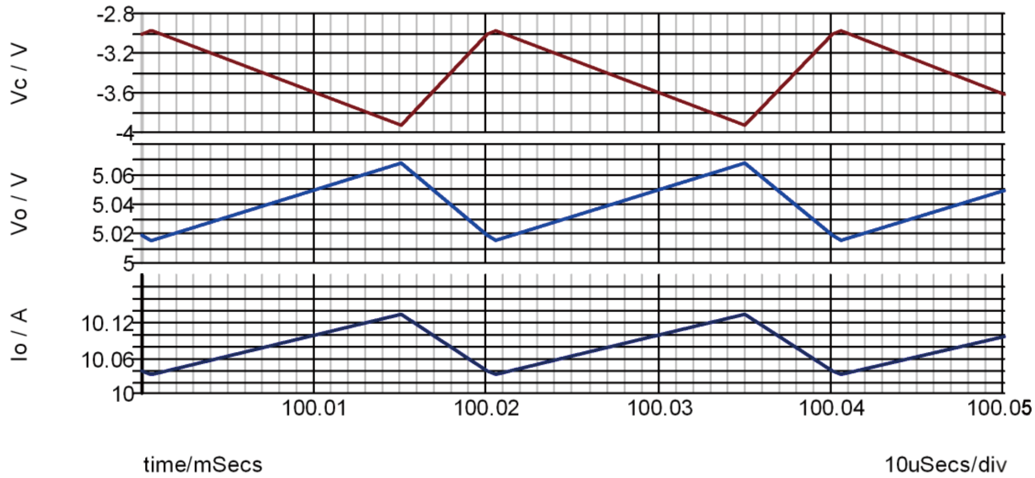

Figure 5. Simulation waveform of v_{c2}, v_o, and i_o under full-load $P_o = 50$ W

has a clamp diode and clamp capacitor can recover energy by leakage inductor. Therefore, the voltage stress on the main power switch can be reduced and low voltage stresses components were selected. Finally, Simplis simulation software is used to demonstrate a converter circuit to prove that this proposed converter can be used as corrector magnet power supply of accelerator machine. Future work is to design a hardware 50 W prototype circuit with 24 V input voltage down to 5 V output voltages which is implemented in laboratory.

Acknowledgment. This work is partially supported by National Synchrotron Radiation Research Center. The authors also gratefully acknowledge the helpful comments and suggestions of the reviewers, which have improved the presentation.

REFERENCES

[1] B. Buyuksarac, O. Agus, Y. Ulgen, H. Bilge and Z. Ozen, Relative dose distribution in gamma knife treatment near tissue inhomogeneties, *Proc. of IEEE IEMBS*, pp.3086-3089, 2006.
[2] G. Janssens, L. Bombelli, E. Clementel, C. Fiorini, L. Hotoiu, R. Peloso, D. Prieels, J. Smeets, E. Sterpin and F. V. Stappen, First acquisitions of realistic proton therapy treatments delivered on an anthropomorphic phantom with a prompt gamma camera, *Proc. of IEEE NSS-MIC*, pp.1-4, 2014.
[3] C. Y. Liu, J. Chiou, Y. C. Chien and C. H. Kuo, Modification of the correction bipolar power supply of the storage ring, *Proc. of IEEE PAC*, pp.764-766, 2003.

[4] F. Marvi, E. Adib and H. Farzanehfard, Zero voltage switching interleaved coupled inductor synchronous buck converter operating at boundary condition, *IET Power Electronics*, vol.9, no.1, pp.126-131, 2016.

[5] R. J. Wai and J. J. Liaw, High-efficiency coupled-inductor-based step-down converter, *IEEE Trans. Power Electronics*, vol.31, no.6, pp.4265-4279, 2016.

[6] P. Xu, M. Ye, P. L. Wong and F. C. Lee, Design of 48V voltage regulator modules with a novel integrated magnetics, *IEEE Trans. Power Electronics*, vol.17, no.6, pp.990-998, 2002.

[7] R. Y. Duan and J. D. Lee, High-efficiency bidirectional DC-DC converter with coupled inductor, *IET Power Electronics*, vol.5, no.1, pp.115-123, 2012.

[8] C. T. Pan, C. F. Chuang and C. C. Chu, A novel transformerless interleaved high step-down conversion ratio DC-DC converter with low switch voltage stress, *IEEE Trans. Industrial Electronics*, vol.61, no.10, pp.5290-5299, 2014.

[9] M. Esteki, B. Poorali, E. Adib and H. Farzanehfard, High step-down interleaved buck converter with low voltage stress, *IET Power Electronics*, vol.8, no.12, pp.2352-2360, 2015.

[10] M. Esteki, B. Poorali, E. Adib and H. Farzanehfard, Interleaved buck converter with continuous input current, extremely low output current ripple, low switching losses, and improved step-down conversion ratio, *IEEE Trans. Industrial Electronics*, vol.62, no.8, pp.4769-4776, 2015.

[11] I. O. Lee, S. Y. Cho and G. W. Moon, Interleaved buck converter having low switching losses and improved step-down conversion ratio, *IEEE Trans. Power Electronics*, vol.27, no.8, pp.3664-3675, 2012.